Earth and Planetary Science Letters 323-324 (2012) 60–71

Contents lists available at SciVerse ScienceDirect

Earth and Planetary Science Letters

journal homepage: www.elsevier.com/locate/epsl

Asthenospheric flow and lithospheric evolution near the Mendocino Triple Junction

Kaijian Liu [a,b,*], Alan Levander [a], Yongbo Zhai [a], Robert W. Porritt [c], Richard M. Allen [c]

[a] Department of Earth Science, MS-126, Rice University, Houston, TX 77005, USA
[b] Applied Physics Program, MS-366, Rice University, Houston, TX 77005, USA
[c] Department of Earth and Planetary Sciences, University of California, Berkeley, CA 94720, USA

ARTICLE INFO

Article history:
Received 20 August 2011
Received in revised form 16 January 2012
Accepted 18 January 2012
Available online xxxx

Editor: P. Shearer

Keywords:
Mendocino Triple Junction
joint inversion
young asthenosphere
slab window
mantle wedge

ABSTRACT

The migration of the Mendocino Triple Junction in northern California creates a complicated lithosphere–asthenosphere boundary system at shallow depths (<60 km), following the progressive transition from Cascadia subduction to San Andreas transform motion. It provides a natural laboratory to examine lithospheric evolution associated with slab removal in an active tectonic setting. However, pathways of the asthenospheric sources that fill the slab-free region created by the triple junction migration remain unclear. Previous active source profiles and body-wave tomography are limited to either crustal or a deeper upper mantle scale, respectively. In this study, we present a three-dimensional shear velocity model from joint inversion of ambient noise (8–30 s) and ballistic Rayleigh wave dispersion curves (22–100 s), as well as Ps receiver functions, using 111 stations from the Flexible Array Mendocino Experiment, USArray Transportable Array and the regional Berkeley Digital Seismic Network. In the crust, we have observed the low-Vs Franciscan Complex in the Coast Ranges and the relatively high-Vs Great Valley ophiolite abutting the low-Vs Sierran basement. The low-Vs uppermost mantle imaged near the sudden steepening of the subducted oceanic slab extends seismic evidence for forearc mantle serpentinization further south along the Cascadia margin. In addition to the asthenosphere beneath the Gorda plate, the joint inversion Vs model further identifies three other young asthenospheres resulting from different partial melting mechanisms. Northward motion of the triple junction causes asthenospheric flow both from under the Gorda plate and from the cooling former mantle wedge left under the Great Valley and Sierra Nevada, imaged from the joint inversion as a relatively deep (>75 km) low-Vs anomaly. These two mantle flows appear to begin mixing ~100 km south of the southern edge of the Gorda plate in the slab window region. We speculate that the latter provides the wedge-type geochemical signature seen in the Coast Range volcanic rocks, reconciling slab window models and volcanic geochemistry. This 'staggered' upwelling model proposed here also explains the ~3 Myr delay in onset of volcanism after triple junction migration.

1. Introduction

The Mendocino Triple Junction (MTJ) is a transform–transform-trench triple junction forming the intersection of the Pacific, North American and Gorda plates in northern California (e.g., Dickinson and Snyder, 1979; Furlong and Schwartz, 2004) (Fig. 1). The MTJ was formed ~25–29 Ma by the impingement of the Pacific–Farallon ridge on the North American trench, initiating San Andreas fault (SAF) strike-slip motion (Atwater, 1970). North of the MTJ, the subduction of the young Gorda plate beneath North America forms the southern terminus of the Cascadia subduction zone. The northwestward migration of the MTJ, resulting in the progressive replacement of the subduction zone by the transform margin, has profoundly altered the lithospheric structure of the western North American plate boundary through a variety of tectonic and magmatic processes (e.g., Dickinson, 1997). The triple junction region has two distinct volcanic systems: the southernmost Cascade Quaternary volcanic centers (e.g. Mount Shasta and Lassen Peak), resulting from mantle wedge melting above the Gorda plate (Leeman et al., 2005) and the northern Coast Range volcanic system, consisting of isolated volcanic centers with northward decreasing ages aligned along the strike of the range, the youngest being the Clear Lake volcanic fields (~2–0.1 Ma) (Dickinson, 1997; Furlong and Schwartz, 2004; Johnson and O'Neil, 1984).

The northwestward migrating MTJ leaves in its wake a lithospheric gap at the southern edge of the Gorda plate (SEDGE) (Dickinson and Snyder, 1979; Furlong and Schwartz, 2004; Levander et al., 1998; Liu and Furlong, 1992), thought to be filled by asthenospheric flow, the subject of this paper. Late-Cenozoic Coast Range volcanism and toroidal mantle flow are attributed to flow into the gap (Eakin et al., 2010; Zandt and Humphreys, 2008). Evidence supporting this model includes surface heat flow (Lachenbruch and Sass, 1980), patterns of volcanism (e.g., Dickinson, 1997), active and passive source

* Corresponding author at: Dept. of Earth Science, Rice University, Houston, TX 77005, USA. Tel.: +1 713 348 5169.
E-mail address: lkjcammit@gmail.com (K. Liu).

0012-821X/$ – see front matter © 2012 Elsevier B.V. All rights reserved.
doi:10.1016/j.epsl.2012.01.020

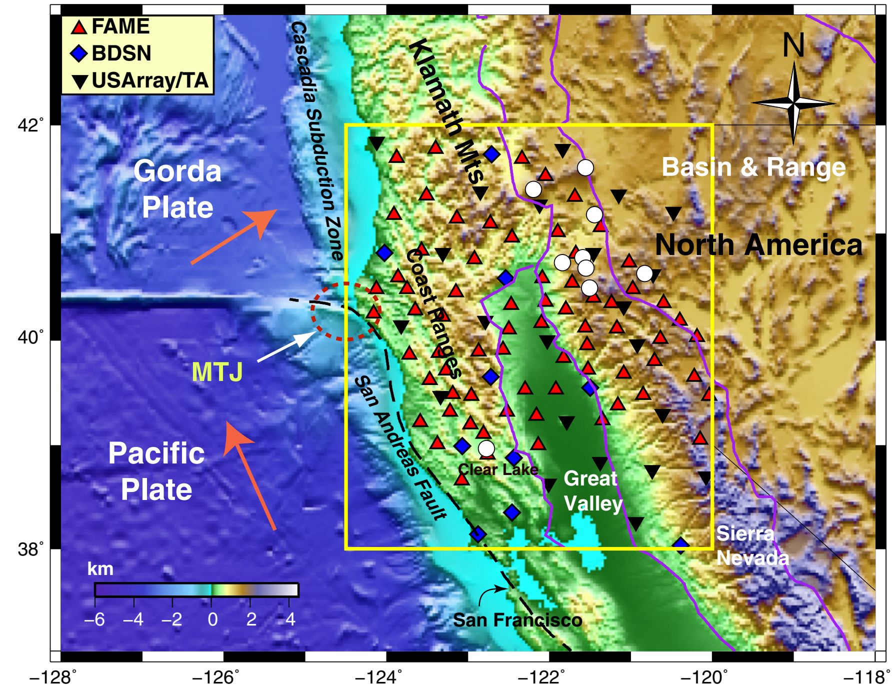

Fig. 1. Study region (yellow box) with topography and principal tectonic features. We analyzed broadband data from 75 FAME stations (red triangles), 22 USArray/TA stations (dark inverse triangles), and 14 Berkeley Digital Seismic Network (BDSN) stations (blue diamonds). Volcanoes are plotted as white dots, including Clear Lake, in the Coast Ranges, and Mt. Shasta and Lassen Peak in the Cascade Ranges. Dark dashed line shows the SAF along the Pacific-North American plate boundary. Purple lines mark the major tectonic boundaries. Orange arrows indicate Pacific and Gorda plate motions relative to North America. (For interpretation of the references to color in this figure legend, the reader is referred to the web version of this article.)

seismic images (Beaudoin et al., 1996; Beaudoin et al., 1998; Benz et al., 1992; Levander et al., 1998; Zhai, 2010), and geodynamic modeling (Liu and Furlong, 1992; Zandt and Furlong, 1982). The origin of the slab window asthenosphere and the flow paths into the gap following slab removal are debated (e.g., Cole and Basu, 1995; Hole et al., 1998; Schmitt et al., 2006; Whitlock et al., 2001). Previous asthenospheric upwelling models fall into two categories, involving either subcontinental (e.g., Johnson and O'Neil, 1984; Liu and Furlong, 1992; Schmitt et al., 2006; Whitlock et al., 2001) or suboceanic (e.g., Cole and Basu, 1995; Zandt and Humphreys, 2008; Zhai, 2010) sources.

Seismic converted wave imaging, tomography, and SKS split times can be used to identify the slab window structure, asthenospheric seismic velocities, and the directions of mantle flow in the MTJ region. In this study, we constructed a three-dimensional shear velocity model by the joint inversion of Ps receiver functions and fundamental-mode Rayleigh wave dispersion data (8–100 s) from the EarthScope flexible and transportable arrays (Fig. 1). The joint inversion provides better vertical resolution of upper mantle structures in the resolution gap that exists from roughly the Moho to the asthenosphere between teleseismic body-wave tomography (Benz et al., 1992; Obrebski et al., 2010; Schmandt and Humphreys, 2010) and active seismic studies (Beaudoin et al., 1996, 1998; Henstock et al., 1997; Levander et al., 1998).

2. FAME and USArray datasets

We used data from the Flexible Array Mendocino Experiment (FAME) network, which consists of 75 broadband seismic stations deployed in northern California from July 2007 to June 2009. Additionally, we incorporated data from 22 USArray Transportable Array (TA) stations and 14 Berkeley Digital Seismic Network (BDSN) stations, as they have temporal overlap with the FAME experiment (Fig. 1). Using a total of 111 stations, we first measured fundamental-mode Rayleigh wave phase velocities (22–100 s). The resulting phase velocities were combined with short-periods (8–30 s) from an ambient noise tomography (ANT) study (Porritt et al., 2011), yielding broader band surface wave dispersion curves (8–100 s). We inverted for the isotropic Vs structure using the joint inversion of the combined dispersion curves and the Ps receiver functions (Zhai, 2010) made with data from the same stations.

2.1. Ballistic Rayleigh wave phase velocity (22–100 s)

We use 224 teleseismic earthquakes with epicentral distance between 30° and 120°, magnitude >5.5 and depths <70 km (Fig. 2a, b). To account for the nonplanar energy in the fundamental-mode Rayleigh wavefield caused by multipathing or small-scale scattering, we applied the modified two-plane wave technique (Forsyth and Li, 2005; Liu et al., 2011; Yang and Forsyth, 2006), which incorporates finite-frequency sensitivity kernels for both amplitude and phase (Yang and Forsyth, 2006). Here, the recorded wavefield is represented approximately by the sum of two interfering plane waves. We inverted the Rayleigh wave phase velocities for 13 frequency bands from 22 to 100 s based on a grid of 0.25°×0.25° near the MTJ region. The combination of the FAME, USArray/TA and the Berkeley BDSN stations provides dense enough coverage to resolve the relatively short wavelength phase velocity variations.

2.2. Ambient noise dispersion data (8–30 s)

Ambient noise tomography computes the cross-correlation waveform of seismic noise between station pairs as an estimate of the Green's functions to extract the inter-station phase (e.g., Bensen et al., 2007; Shapiro et al., 2005; Snieder, 2004; Yao et al., 2006). The ANT provides shorter-period dispersion data (8–30 s) than the ballistic earthquake tomography described above, which greatly increases the study's sensitivity to crustal shear velocity (Porritt et al., 2011). In the overlapping period range (22–30 s), there is good consistency between the ballistic and ANT phase velocities (Fig. 3c).

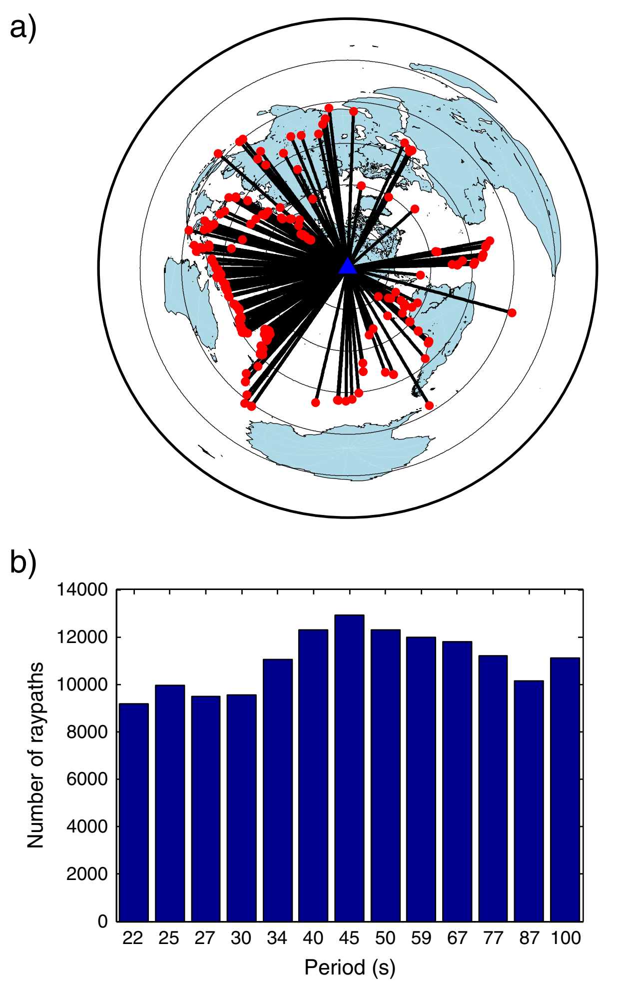

Fig. 2. (a) Azimuthal and distance distribution of the 224 teleseismic events (red dots) for the finite-frequency Rayleigh wave tomography. (b). Number of raypaths for each period (frequency) band from 22 to 100 s in the surface wave study. (For interpretation of the references to color in this figure legend, the reader is referred to the web version of this article.)

2.3. Ps receiver function

We include the Ps receiver functions (1 and 2 Hz), generated using FAME data (Zhai, 2010), in a joint phase velocity/receiver function inversion to provide a stronger constraint on seismic discontinuity structure in the crust and upper mantle. The station-gather receiver functions were made from 186 teleseismic events ($35° \leq \Delta \leq 90°$, Mw > 5.7) using time-domain iterative deconvolution technique (Ligorria and Ammon, 1999). In our joint inversion, we selected two overlapping frequency band receiver functions with hi-cut frequencies of 1 and 2 Hz (corresponding Gaussian widths of 2.07 and 4.14, respectively). The receiver functions increase sensitivity to the underlying seismic discontinuity structure, while use of two different frequencies improves our ability to differentiate between first order discontinuities and Vs gradients, which both cause P-to-S conversions (e.g., Julia et al., 2000). To enhance the signal-to-noise ratio, we divided the receiver functions under each station into three groups with different ray parameters (<0.05 s/km; 0.05–0.06 s/km; >0.06 s/km). After the Ps time move-out correction (e.g., Rondenay, 2009) was applied and assuming the 1-D background Tectonic North America (TNA) shear model (Grand and Helmberger, 1984), we stacked the three groups of receiver functions individually at the central ray parameters of 0.045, 0.055 and 0.065 s/km, as well as collectively at 0.05 s/km (e.g., Fig. 3a). This stacking technique reduces sensitivity to deep discontinuities and crustal reverberations while enhancing the shallow conversion signals; therefore, we used short time windows from −5 to 10 s (equivalent to about 100 km depth) for both low and high frequency receiver functions (Fig. 3a and S1b). The short windows prevent modeling multiple reflections in the inversion. In this region crustal thickness varies rapidly laterally and vertically in both coast normal and coast parallel directions. Crustal multiples are poorly predicted by simple 1-D models in the presence of rapid crustal thickness changes. The significant signals for our study, the Moho and lithosphere–asthenosphere boundary (LAB), are contained within the first 10 s after P, since LAB depths in this region are typically <100 km (Li et al., 2007; Zhai, 2010).

3. Joint inversion method

To reduce the nonuniqueness of the Vs inversion from each single dataset, we jointly invert the shear-velocity structure beneath each station from the three independent observations (e.g., Fig. 3): (1) 22–100 s phase velocity from finite-frequency Rayleigh wave tomography, (2) 8–30 s phase velocity from ambient noise tomography (Porritt et al., 2011), and (3) Ps receiver functions at low (1 Hz) and high (2 Hz) frequency bands (Zhai, 2010). The dispersion curves from the first two observations provide complementary constraint on the average absolute Vs from the shallow crust to the upper mantle, while the Ps receiver functions are primarily sensitive to the shear impedance variations with depth. The combined constraints significantly decrease the nonuniqueness of the Vs inversion, and thus improve the model reliability for the crust and upper mantle (Fig. 4). The joint inversion also helps refine Moho and LAB depth estimates in regions of ambiguity in the receiver function images (Fig. 5a, b).

We used the Computer Programs in Seismology package (Herrmann and Ammon, 2002) to invert the 1-D shear velocity models beneath the 111 stations (Fig. 3). We modified the cost function here to include all three datasets with assigned weight for the joint inversion:

$$\frac{1-p}{N_{rf}N_{pts}}\sum_{i=1}^{N_{rf}}\sum_{j=1}^{N_{pts}}\|\varepsilon_{ij}^{rf}\|^2+\frac{p}{N_{dsp}}\left\{w_{RWT}\sum_{i=1}^{N_{RWT}}\|\varepsilon_i^{RWT}\|^2+w_{ANT}\sum_{i=1}^{N_{ANT}}\|\varepsilon_i^{ANT}\|^2\right\} \quad (1)$$

where $\varepsilon_i \equiv (d_i^{OBS}-d_i^{PRE})/\sigma_i$ is the relative residual between the observed and synthetic data, N_{rf}, N_{dsp}, N_{RWT}, N_{ANT} are the total numbers of receiver functions, periods at which dispersion was measured, Rayleigh wave ballistic phase velocities, and ANT phase velocities, respectively. N_{pts} is the total number of sampling points in each receiver function, and p is the influence factor controlling the constraining weight given to the receiver function data and the dispersion data (Fig. S1a). In order to avoid overemphasis of the ambient noise data due to closer period sampling, we assigned different weights to the dispersion data from earthquake tomography and ambient noise analysis in the form of $w_i = N_{dsp}/2N_i(i = RWT, ANT)$. Thirty iterations were used for the nonlinear inversion for the Vs model starting from the TNA reference model with no *a priori* crustal structure (Fig. 3b). A slight increase of the weight term at the Moho depth estimated from the receiver functions allowed the possibility of large velocity variations under smoothing regularization. If the *a priori* Moho depth differs greatly from the true model, the iterative inversion will search for the true depth. The joint inversion also helps to improve the Moho and LAB depth estimates with respect to those made from receiver functions alone (Fig. 5).

After completion of the station-by-station joint inversion for 1-D Vs structure, the 1-D profiles were collected into a 3-D volume and interpolated onto a regular horizontal and vertical grid. Although the interpolation smoothes out sharp velocity changes, the lateral resolution in the 3-D volume is as good as the station spacing (~35 km) allows. The horizontal resolution is controlled by a number of factors,

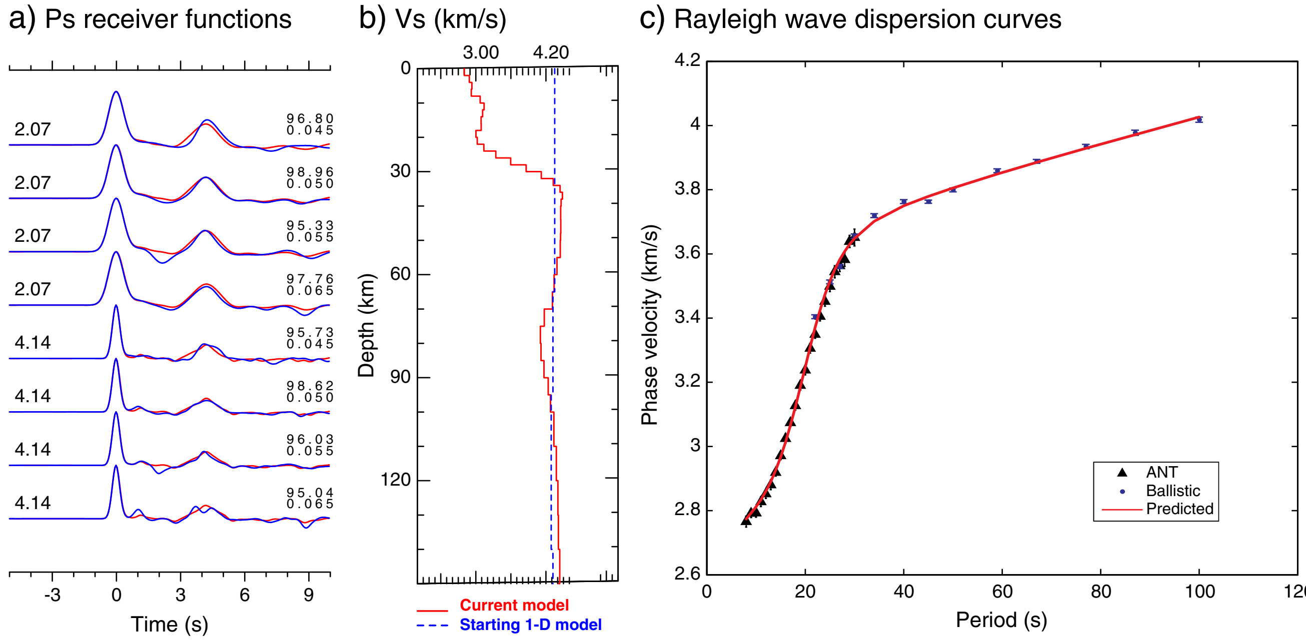

Fig. 3. One example of a Rayleigh wave-receiver function joint inversion at station XQ.ME39. (a) We use 1 and 2 Hz Ps receiver functions binned at 0.045, 0.050, 0.055 and 0.065 s/km. Red and blue are the predicted and observed receiver functions, respectively. Top four traces are the 1 Hz receiver functions, and bottom four are the 2 Hz receiver functions. Each trace includes Gaussian filter parameters on the left, and percentage of model fit and ray parameter on the right. (b) The starting Vs model for the joint inversion is a constant velocity using the uppermost mantle velocity from the Tectonic North America (TNA) model (dashed blue line) with no *a priori* information for the crustal thickness and velocities. Red line is the final Vs model after 30 iterations. (c) Both ANT (dark triangles) and ballistic (blue dots) Rayleigh wave phase velocities are used in the joint inversion, while the predicted dispersion curve (red) is calculated from the final Vs model from (b). (For interpretation of the references to color in this figure legend, the reader is referred to the web version of this article.)

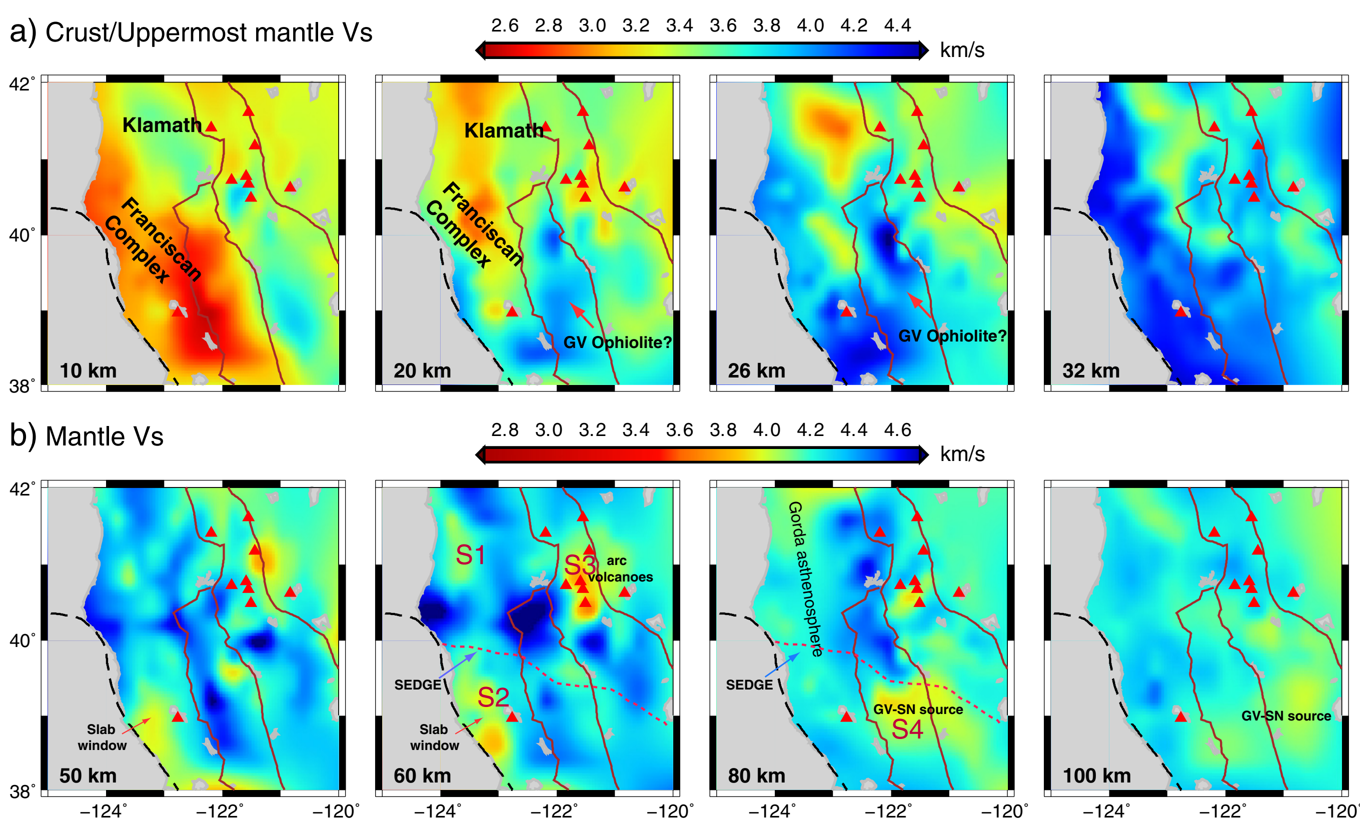

Fig. 4. Shear velocity maps at depths from 10 to 100 km from the joint inversion of ambient noise, ballistic Rayleigh wave dispersion and Ps receiver functions. Red triangles are the volcanic fields. Dark dashed line is the San Andreas Fault. The red dashed line is the inferred SEDGE. Note that the crust/uppermost mantle (a) and upper mantle (b) velocity maps are plotted with different color scales.

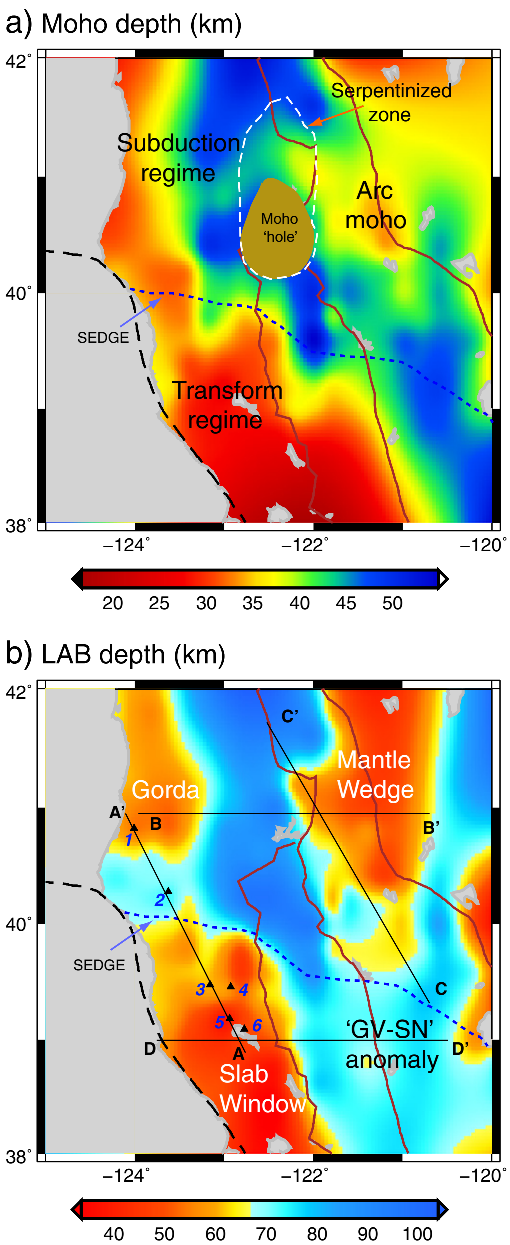

Fig. 5. Estimated (a) Moho and (b) LAB depth maps. Blue dashed line marks the SEDGE. The relative thick forearc crust refers to the oceanic Moho. The white dashed line in (a) outlines the serpentinized zone, where we observe low-Vs uppermost mantle. Dark thin lines (AA′, BB′, CC′ and DD′) in (b) show the locations of cross-sections shown in Fig. 6 and 7. The numbers 1–6 identify the locations of the Vs-z profiles in Fig. S4. (For interpretation of the references to color in this figure legend, the reader is referred to the web version of this article.)

including the wavelengths of the surface waves used in the tomography, the assumption that all the signals can be described by two-plane waves (resolution estimated as inter-station spacing of ~35 km for periods <40 s) (Yang et al., 2008), and the 1-D inversion. Vertical resolution is controlled by a combination of the Rayleigh wave's vertical averaging of velocity, the receiver functions' ability to identify sharp gradients, and the weight given to each in the inversion (Fig. S1a). For the dispersion data, the constraint on the absolute Vs at different periods decays with depth, with the sensitivity peaks located at depths of approximately a third of a wavelength (e.g., Liu et al., 2011). The receiver function's vertical resolution is no better than ¼ of a wavelength; therefore, for a frequency of 1 Hz, a shear wave at the Moho would be unable to distinguish between an impedance (shear velocity times density) gradient occurring over about 1 km and a step in impedance.

4. Result and discussion

4.1. Crustal heterogeneity: Franciscan Complex, ophiolite, and crustal melt

The crustal heterogeneity revealed by the joint inversion Vs model correlates well with surface geological features and reflects the complicated tectonic history in the accretionary wedge near the continental margin. The upper crustal low-Vs values (<3.0 km/s) in the Coast Ranges (Fig. 4a) are Franciscan Complex accretionary wedge, low to high-grade metamorphic rocks (e.g., Blake et al., 1985). Along the Coast Range Fault (10 and 20 km depth, Fig. 4a), the Franciscan Complex is juxtaposed against the Klamath block, which has higher velocities (3.4–3.6 km/s), reflecting the Trinity ultramafic sheet and North Fork ophiolite (Thurber et al., 2009; Zucca et al., 1986). The low-velocity layer underlying the Klamath block is most likely accretionary wedge sedimentary rocks, or possibly peridotite serpentinized under low-temperature conditions. In the Great Valley, the shallow low-Vs layer is an average of the thick sedimentary basin and the underlying crust, since we do not account directly for the basin in the starting model. The underlying high-velocity body in the valley (20 and 26 km depth, Fig. 4a) is interpreted as the Great Valley ophiolite, probably resulting from back arc obduction of oceanic crust/mantle over the continental material during the Jurassic orogeny (Godfrey and Klemperer, 1998). The ophiolite under the Great Valley can be distinguished from the lower Vs Sierran basement which is either the Foothills Metamorphic Complex and/or the intrusive batholith (Godfrey and Klemperer, 1998; Godfrey et al., 1997). Under the Cascadia volcanoes such as Lassen Peak and Mt. Shasta, the pronounced low-velocity layer (Vs~3.0 km/s) in the crust (e.g. Fig. 4a) suggests crustal partial melt above the mantle wedge.

4.2. Comparison with MTJSE Line 9

The MTJ marks the transition from a subduction (convergent) regime to a transform regime resulting from the northward migration of the Pacific and Gorda plates relative to North America, which profoundly influenced North American lithospheric structure (Beaudoin et al., 1996, 1998; Dickinson and Snyder, 1979; Furlong and Schwartz, 2004; Henstock et al., 1997; Levander et al., 1998). We compare our joint inversion Vs cross-section with the corresponding receiver function image (Zhai, 2010) and the crustal reflection/refraction P-wave velocity models (Beaudoin et al., 1996, 1998), along Line 9 from the MTJ Seismic Experiment (MTJSE) (Fig. 6a–c).

4.3. Gorda plate

At the northern end of the profile, the high-Vs body (3.6–4.5 km/s; Fig. 6c) is the subducting Gorda plate. The SEDGE is reasonably well defined as the limit of high velocities to the south, marking the youngest part of the slab-free region in the transform regime near x = 90 km (Fig. 6). The high Vs region indicative of the plate is bounded above by a positive receiver function event, and below by a negative event. The former, a broad pulse, we interpret as interfering signals from the oceanic Moho and top of the oceanic crust (~20–25 km). The top of the oceanic crust in the Vs image is consistent with strong reflections from the active source study (Fig. 6a). The Gorda oceanic crust appears as intermediate velocities (~3.9–4.1 km/s) between the reflections from the top of the crust and the Moho (dark and white lines in Fig. 6b, respectively). The negative receiver function signal at the bottom of the high velocity plate (~4.4–4.5 km/s) we interpret as the Gorda LAB at ~70 km. The

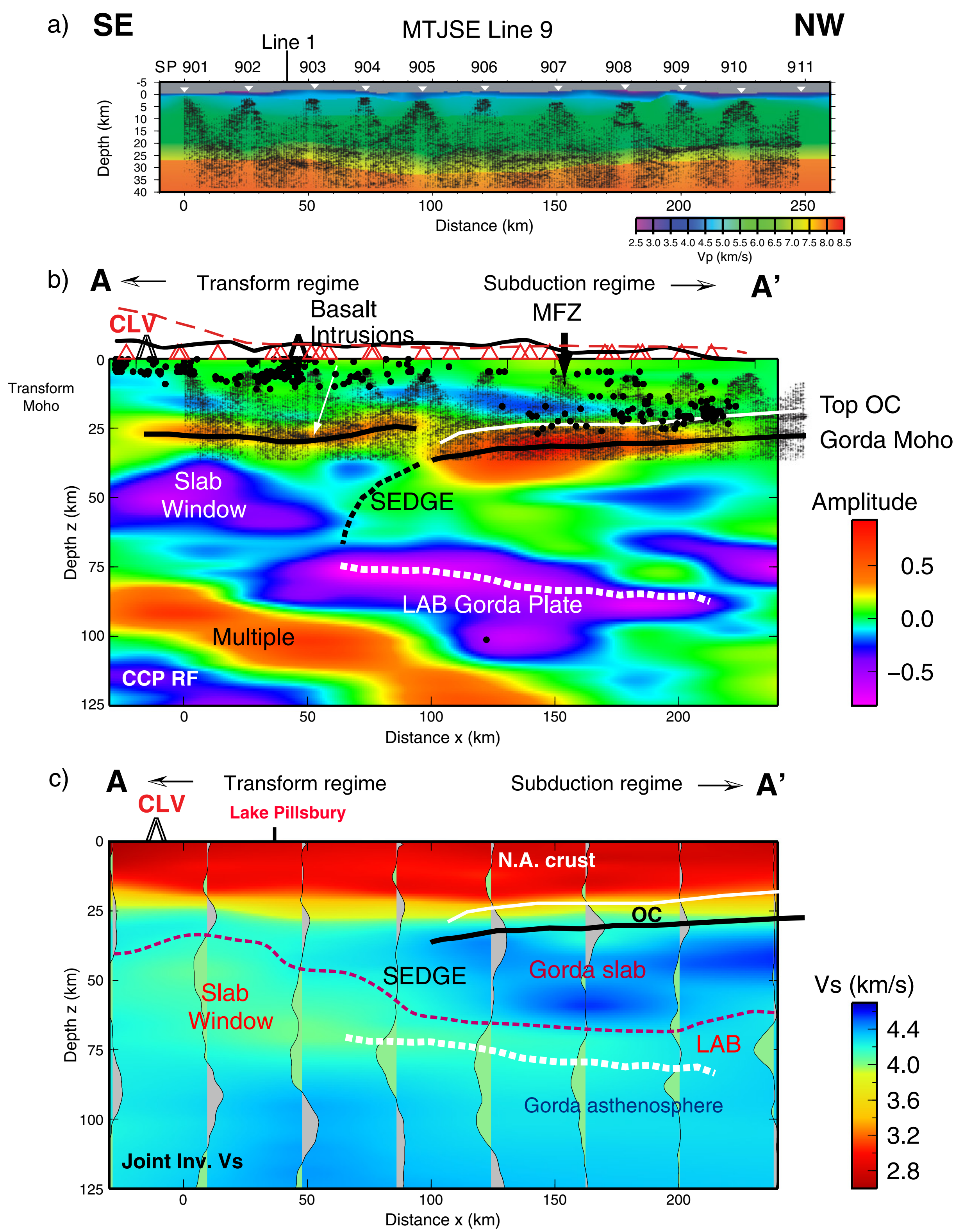

Fig. 6. Comparison of cross-sections from the joint inversion Vs model with other seismic results along the MTJ Seismic Experiment (MTJSE) Line 9 (A-A′ in Fig. 5b). (a) A crustal Vp model similar to that of Beaudoin et al. (1996), (b) Ps receiver function image (Zhai, 2010), and (c) the joint inversion Vs model. Dark dots in (b) are earthquake hypocenters. In the joint inversion Vs image (c), we superimpose the top of the oceanic crust (OC) (white solid line), Gorda Moho (dark solid line), and the LAB depth under the Gorda plate (white dashed line) determined from the active source model and FAME receiver functions. Purple dashed line is the estimated LAB from the joint inversion Vs model taken as the center of the negative Vs gradient. (For interpretation of the references to color in this figure legend, the reader is referred to the web version of this article.)

heterogeneous velocity structure within the Gorda lithosphere coincides with the location of the strong internal deformation as indicated by seismicity and seafloor fault offsets (Gulick et al., 2001; Wilson, 1986, 1989). The Gorda plate dips southward toward the MTJ, terminating under the thickest accretionary wedge, also at x = ~90 km (Fig. 6c). It has been hypothesized that mechanical coupling between the slab and the overlying crust cause an ephemeral crustal root to form near the SEDGE (Figs. 6c and S4) (Beaudoin et al., 1998; Furlong et al., 2003).

North of the MTJ, we clearly image the subducting Gorda plate (high-Vs body in Figs. 4b, 6c, 7a) beneath North America. The forearc crust thickens eastward from ~25 to ~40 km, with thickening terminating at the location of rapid plate steepening from ~10° to ~25° dip (Fig. 7a). The estimated plate thickness (~30–40 km) from the receiver function and joint inversion Vs model agrees well with the thickness predicted from the half-space cooling model for oceanic lithosphere (~29–36 km), using ~8–13 Ma as the age of subducted Gorda plate, and 1100 °C as the temperature at the base of the thermal boundary layer and 1300 °C as the (convecting) ambient mantle, respectively. West of the change in slab dip, we observe a shallow LAB (~50–60 km) at the base of the Gorda plate. Low-Vs (<4.2 km/s) in the Gorda asthenosphere is likely due to proximity to the Gorda ridge, and/or shear melt (Kawakatsu et al., 2009) at the base of the subducted slab.

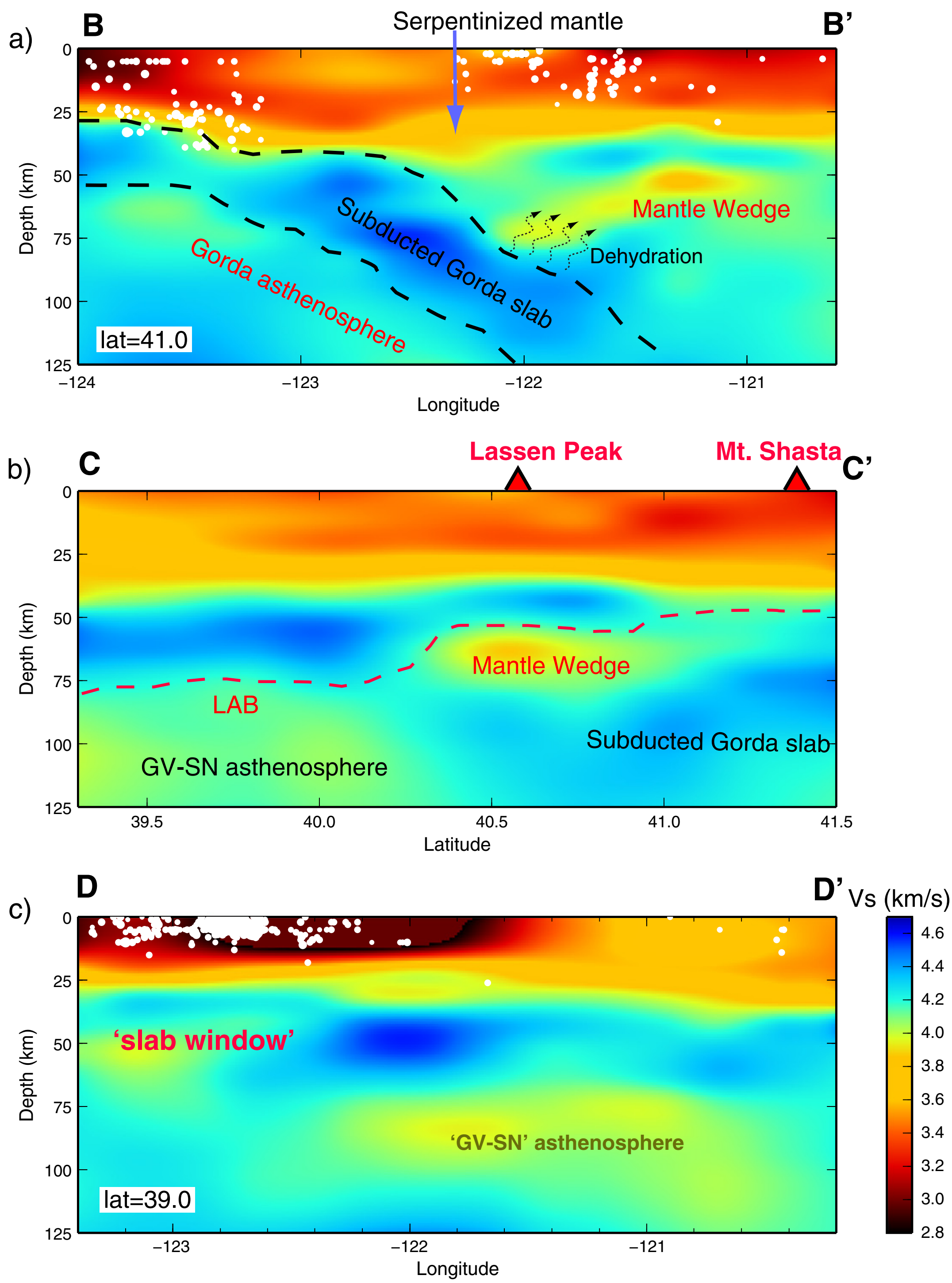

Fig. 7. Vs cross-section along lines B-B′, C-C′, and D-D′ in Fig. 5b. (a) Shows the subducted slab, serpentinized forearc mantle, and low Vs mantle wedge. (b) Under the Cascadia volcanoes, the low Vs mantle wedge lies above a high-Vs body we interpret as the subducted Gorda plate. The 'GV-SN' asthenosphere is relatively deep (>75 km) in comparison to the mantle wedge asthenosphere. (c) Shows the asthenospheric flow from the 'GV-SN' anomaly to the slab window from east to west. White dots in (a) and (c) are the seismicity distribution.

4.4. Slab-free window

In the transform regime, we interpret the shallow low-velocity body between x = 0–80 km at 35–75 km depth as asthenosphere in the slab-free region (Figs. 4b and 6c). North of about x = 50 km, the sub-Moho shear velocity in the 'slab-free window' is <4.2–4.3 km/s but velocity decreases (<4.0 km/s) moving southward between x = 0–50 km. The lowest velocities are at ~35 km depth beneath the Clear Lake volcanic field (Figs. 6c and S4). The continuity of the low velocity anomaly from beneath Gorda to the transform regime would allow mantle flow of sub-Gorda asthenosphere into the slab window. The significant decrease in velocity accompanying this also suggests generation of a small fraction of partial melt.

In addition to the Clear Lake volcanic field, beneath the Lake Pillsbury region, the MTJSE active seismic data have imaged highly reflective bodies in the lower crust, interpreted as partially molten basalt sills (Levander et al., 1998). The area has been the site of midcrustal seismicity interpreted as diking events (e.g., Furlong and Schwartz, 2004). The LAB in the slab-gap region (at z ~ 30–40 km) is 30–45 km shallower than that beneath the Gorda plate (z ~ 60–75 km), resulting in decompression melting of ascending asthenosphere from beneath Gorda. Pressure-released basaltic melt can be generated at the base of the transform crust (Henstock and Levander, 2000), causing the slab window magmatism at Lake Pillsbury and Clear Lake. However, the apparent thickening asthenosphere and thinning of the lithosphere southward away from the MTJ are of the exact opposite the geometry predicted by the simple slab window model as described by Dickinson and Snyder (1979). We suggest that the asthenosphere thickens to the south by upward and lateral flow of hydrated mantle wedge, left behind as the triple junction migrates, as we describe further below.

4.5. Forearc serpentinization

Near the northernmost Great Valley, we detect weak or absent Ps Moho signals, and a complicated Vs structure at the base of the crust, which we term a 'Moho hole' (Figs. 5a and S3) (Zhai, 2010). Serpentinization of the forearc upper mantle has been widely inferred to extend north along the Cascadia margin, where it is characterized by low uppermost mantle Vs, weak or reversed Ps conversions (Bostock et al., 2002), weak or missing P_mP/P_n signals (Beaudoin et al., 1996, 1998; Brocher et al., 2003), and characteristic magnetic anomalies (Blakely et al., 2005). Using the Vs-serpentinization relation (Bostock et al., 2002), the uppermost mantle Vs (~3.7 km/s at ~40 km depth, Fig. 7a) gives an estimate of up to ~30–40% serpentinization of the northern California forearc, an intermediate value between that suggested for Cascadia (Bostock et al., 2002) to the north and a more normal, apparently unserpentinized northern Great Valley ophiolite (Godfrey and Klemperer, 1998) to the south. The transition of serpentinized-to-unserpentinized mantle near the SEDGE suggests further mantle dehydration in the post-subduction regime following slab removal (Fulton and Saffer, 2009), and recycling of the oceanic slab-derived components into the continental mantle. At ~50–75 km, low velocities immediately east and above the subducting Gorda plate (Fig. 7a) suggest the possibility of ongoing dehydration of the plate (e.g., Hacker et al., 2003).

4.6. Young asthenospheres

To the south, the absence of the high-Vs slab defines the SEDGE, similar to body-wave tomography results (Obrebski et al., 2010). Besides the Gorda asthenosphere (S1 in Fig. 4b), we observe three additional low-Vs regions (S2, S3, and S4 in Fig. 4b) in the upper mantle, and identify three modern shallow LABs (Fig. 5b), corresponding to the Cascadia mantle wedge (S3), the San Andreas transform margin (S2), and another low-Vs region (S4), the 'GV-SN' anomaly that we describe below. The SAF LAB shallows rapidly from the subduction regime to <50 km depth beneath Clear Lake. To the east of Clear Lake at greater depths (>75 km) we find low velocities (<4.1 km/s) under the Great Valley and the western Sierra Nevada block, which we term the "GV-SN" anomaly. We interpret this feature as the cooling former mantle wedge. The LAB at the top of the wedge is deeper (~75 km) than elsewhere, likely due to development of a conductively cooling boundary layer and/or a remnant lithospheric lid under North America.

4.6.1. Mantle wedge and Cascadia volcanoes

We interpret the shallow mantle wedge LAB under the Cascadia arc as resulting from hydration-induced decompression melting, causing a significant drop in Vs (Leeman et al., 2005). The extremely low velocities (~3.6 km/s at 60–80 km depth) in the wedge (Fig. 4b and 7a, b) can be attributed to partial melts from dewatering of the subducting oceanic lithosphere and convective upwelling (Leeman et al., 2005). Cross-sections at 41.0 N (Fig. 7) and 40.6 N (Fig. S2) show continuous low velocities from the top of the Gorda plate at 50–75 km depth to directly beneath the Cascadia arc, suggesting that these are fluid pathways from the dehydrating slab. Fluid-mediated decompression melting significantly shallows the LAB depths to 50–60 km, slightly subcrustal, and drives Cascadia magmatism by allowing melt to infiltrate the base of the North American lithosphere. The mantle wedge magmatism causes the arc volcanoes of the southernmost Cascadia Range: Lassen Peak and Mount Shasta. We interpret the low Vs upper mantle in the back arc as a continuation of the mantle wedge asthenosphere.

4.6.2. 'GV-SN' anomaly

As the MTJ migrates northwestward, it leaves behind a mantle wedge. We suggest that the 'GV-SN' anomaly is the former mantle wedge, located to the south, along strike with the current mantle wedge. However, we note that the LAB at ~75 km is deeper than the active mantle wedge by 15–20 km. We interpret the southeastward thickening high-Vs lithospheric lid (~10–30 km thick, Fig. 7b) as a growing thermal boundary layer caused by cooling of former mantle wedge asthenosphere south of the SEDGE.

Slab removal changes the mantle flow field by removing the driving force of mantle wedge counter flow. If the asthenosphere under the Gorda plate can flow into the slab-free window, then Gorda asthenosphere beneath deeper parts of the subducting slab can also flow into the former mantle wedge. It seems likely that the former mantle wedge can also flow laterally and upward into the slab window. The GV-SN low velocity region is likely either, former mantle wedge, or former mantle wedge mixed with Gorda asthenosphere.

4.6.3. SAF transform regime

Beneath the transform regime, the significant decrease in Vs (<4.0–4.2 km/s, Figs. 4b and 6c) and very shallow LAB (~30–40 km) south of SEDGE are attributed to partial melts produced by decompression melting of upwelling asthenosphere from beneath Gorda (Henstock and Levander, 2000). The melting mechanism here differs from that beneath the Gorda plate (shear lensing) and mantle wedge (hydration-induced reduction of the solidus). A certain amount of the melt is accreted at the base of the transform crust (Levander et al., 1998), creating some of the slab window magmatism in Clear Lake and elsewhere in the Coast Ranges. The shallowest LAB under the Coast Ranges is between Clear Lake and Lake Pillsbury, the latter being predicted as a location for future volcanism (Levander et al., 1998). We interpret the continuity of low velocities (Fig. 6c) and SKS split patterns (Fig. 8) to indicate mantle flow into the Coast Ranges slab window from beneath the Gorda plate and from the mantle wedge.

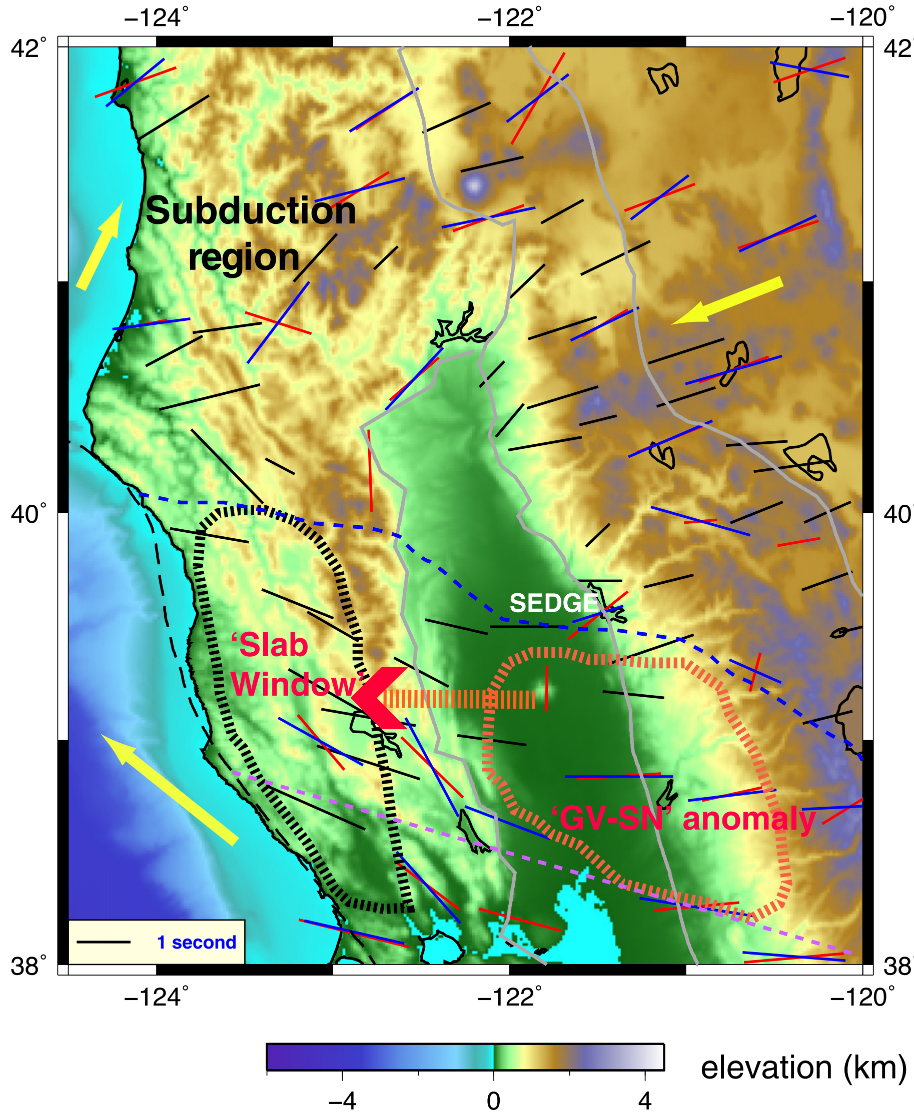

Fig. 8. Fast polarization directions of SKS splits in the MTJ region with absolute plate motions (yellow arrows) of Gorda, Pacific and North American plates. Shear wave splitting results are plotted as different colors: dark from Eakin et al. (2010), blue from Fouch and West (in preparation) and red from Liu (2009). Dark and orange dashed contours are the slab window region in the transform regime and the "GV-SN" anomaly inferred from joint inversion in this study. Blue dashed line is the current SEDGE as shown in Fig. 5, while purple dashed line shows previous SEDGE location. (For interpretation of the references to color in this figure legend, the reader is referred to the web version of this article.)

4.7. Mantle flow

Geochemical data from the northern Coast Range volcanics show strong similarity to the mantle wedge, both having enriched large-ion lithophile and depleted high-field-strength elements (e.g., Furlong and Schwartz, 2004; Whitlock et al., 2001). Hole et al. (Hole et al., 1998) argued that a mantle wedge-derived origin could better fit the Coast Range heat flow data (Lachenbruch and Sass, 1980), i.e., mantle flow from the wedge to the shallow slab-free region. In contrast, initially low $^{87}Sr/^{86}Sr$ ratios and high ε_{Nd} of the volcanic rocks (Cole and Basu, 1995) in the Coast Ranges south of Clear Lake imply that the slab window was first occupied by asthenosphere from an oceanic source. This is consistent with the continuity of the LAB topography in the slab window south of the SEDGE (Zhai, 2010).

It has been suggested that a circular pattern of SKS splits observed in central California, Nevada, Utah and Oregon result from large scale toroidal mantle flow emanating from beneath the Gorda plate along the SEDGE (e.g., Eakin et al., 2010; Zandt and Humphreys, 2008). The scale of this flow pattern is almost entirely out of our study region. For example Fig. 1 of Piromallo et al. (2006) and Fig. 2b of Zandt and Humphreys (2008) suggest that immediately south of the MTJ, mantle flow from under the sinking Gorda plate will be normal to the plate edge, meaning to the south-southwest in the Mendocino region, and of small magnitude. SKS splitting measurements from Eakin et al. (2010), Liu (2009) and Fouch and West (in preparation) show a nearly SEDGE parallel signature (Fig. 8) with relatively large magnitudes (~1 s). The inconsistency between the observed SKS splits in the MTJ region and the predictions of toroidal flow are the result of the scale of observation. We suggest that locally the plate edge causes a more complicated mantle flow field as the sinking plate drags viscous mantle down with it.

The low Vs in the GV-SN anomaly, the SKS splits, and the appearance of a mantle wedge signature in the geochemical data (Whitlock et al., 2001) lead us to hypothesize a 'staggered', two-stage upwelling model (Figs. 9 and 10). We suggest that as North America moves to the northwest, the opening slab window is filled from two sources: The sub-Gorda asthenosphere flows upward and to the southeast into the slab window, while simultaneously abandoned mantle wedge flows upward and to the southwest into the slab window (Figs. 9 and 10b, c). The abandoned wedge is left behind as the 'GV-SN' asthenosphere (Figs. 7c and 8), and is likely still contributing to the slab window asthenosphere by upward and lateral flow. The

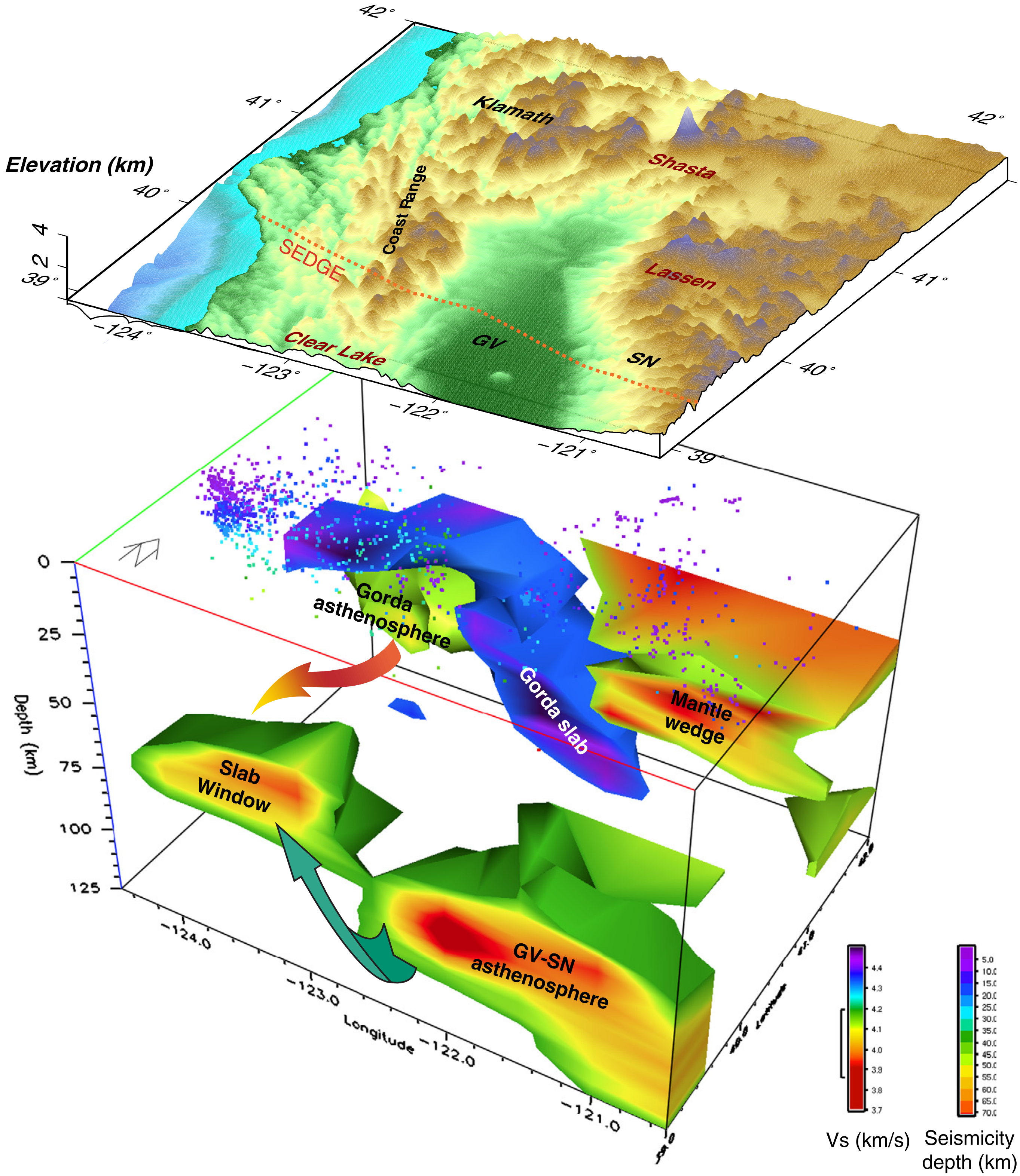

Fig. 9. The 'staggered upwelling' model illustrated by the Vs isosurfaces (3.86, 4.20, and 4.35 km/s) at 39–40°N and 41–42°N, overlain by the topography map. We suggest a hybrid source for asthenospheric upwelling near the SEDGE (dashed orange line in the topography map), first infilled by the subslab source (red arrow) after slab removal, followed by the major flow (green arrow) from beneath the 'GV-SN' anomaly in its east. The colored dots indicate the location of the seismicity in the 41–42°N region. (For interpretation of the references to color in this figure legend, the reader is referred to the web version of this article.)

former mantle wedge still retains a large amount of slab-derived fluids that can suppress the solidus temperature, producing decompression melting as it ascends, causing surface volcanism and the significant Vs reduction under Clear Lake (Figs. 6c and 9). The 'GV-SN' asthenosphere provides the mantle wedge-type geochemical signatures (e.g., Whitlock et al., 2001). The SKS split directions are consistent with southeast flow from beneath Gorda, southwest flow from beneath Cascadia, and east to west flow from the GV-SN anomaly.

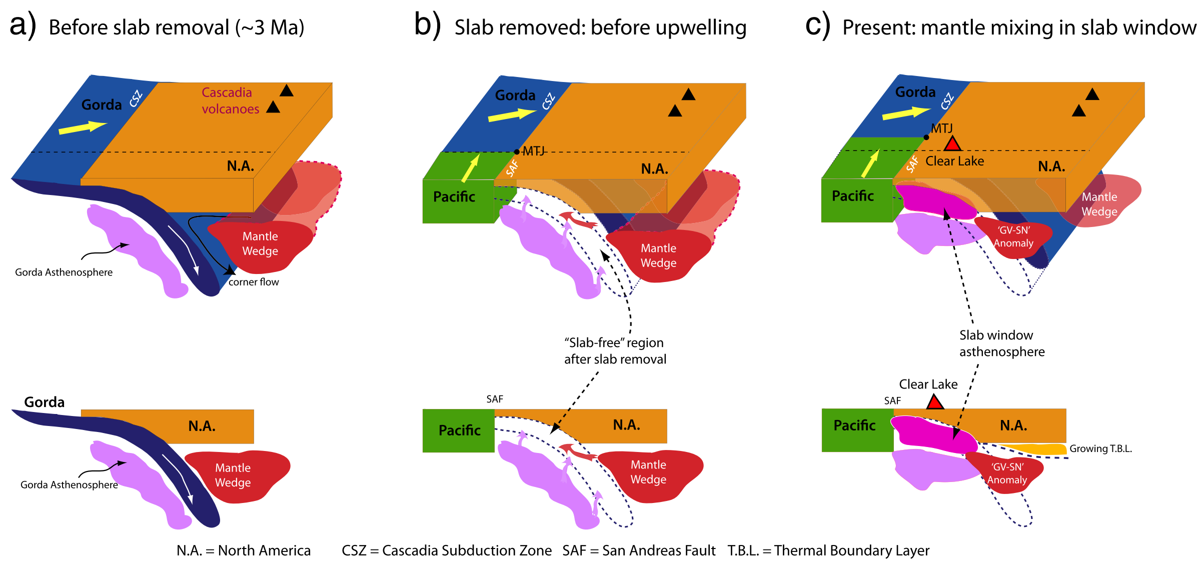

Fig. 10. Schematic diagrams of mantle upwelling model under the transform regime. North American plate is fixed. Bottom figures are cross-section views taken along the latitude of Clear Lake, shown as the dark dashed lines in the top panel. (a) The MTJ was in south of the current Clear Lake location, as the Gorda plate was subducting beneath the North American lithosphere along the Cascadia subduction zone, forming the Cascadia arc volcanoes (dark triangles). The Gorda asthenosphere was separated from that of the mantle wedge by the subducting plate. (b) An imaginary moment right as the subducting slab passes the MTJ and is replaced by asthenosphere. Northward migration of the Gorda plate creates the slab-free region. The Gorda and mantle wedge asthenospheres start to upwell and mix in the slab-free window region. (c) After mantle upwelling and mixing. Decompression melting led to the most recent surface volcanism at Clear Lake in the Coast Ranges. The abandoned mantle wedge is the "GV-SN" anomaly (red), which contributes hydrated mantle wedge asthenosphere to the melting region under Clear Lake. (For interpretation of the references to color in this figure legend, the reader is referred to the web version of this article.)

This wedge-to-window mantle flow is consistent with numerical simulation based on the MTJ geometry under the transform regime (Liu and Furlong, 1992), as well as several other studies (e.g., Furlong and Govers, 1999; Furlong and Schwartz, 2004; Guzofski and Furlong, 2002). The east–west Vs cross-sections (Fig. S2) show that the low-velocity asthenosphere is continuous from the 'GV-SN' anomaly to the low velocities of the slab window under the Coast Ranges, consistent with this asthenospheric flow model.

This model also provides an alternative explanation for the notable time lag (~3 Myr in Clear Lake) between MTJ migration and Cenozoic Coast Range volcanism (e.g., Dickinson, 1997). Although part of the delay in northern Coast Range volcanism could be caused by time spent establishing a magmatic system (Dickinson, 1997; Liu and Furlong, 1992), or the propagation time of the flow from the arc to the window (Furlong and Schwartz, 2004), the staggered upwelling model suggests that the delay in volcanism results from the times of vertical and lateral transport of the former wedge into the slab window, and mixing with the Gorda asthenosphere. Until there is sufficient accumulation of hydrated asthenosphere at shallow depths to dramatically suppress the mantle solidus and enable large scale decompression melting, volcanism is limited to small-volume decompression melting of Gorda asthenosphere (Henstock and Levander, 2000; Levander et al., 1998).

5. Conclusions

Overall, a variety of seismic probes identify four distinct, young LABs and indicate mantle flow between them in the MTJ region. Joint inversion of Rayleigh wave phase velocity dispersion data (8–100 s) and Ps receiver functions provides complementary constraints on the Vs structure at the lithospheric scale. The relative plate motions associated with the northwestward migration of the MTJ produces three distinct modern asthenospheres: one beneath the volcanic arc where dewatering continues, one remnant mantle wedge in which fluid flux has stopped, and the long-discussed slab window beneath the Coast Ranges. We suggest that the slab window is filled by mantle material from the Gorda asthenosphere and from the present and abandoned mantle wedge. The fourth LAB is under the subducting Gorda plate. These four young LABs are strongly related to subduction (vertical) and northwestward (horizontal) migration of the MTJ. The 'staggered' upwelling model, which mixes mantle flow from beneath the Gorda plate and with that from the mantle wedge, is consistent with the seismic observations, and identifies the source of the mantle-wedge geochemical signature seen in the Clear Lake volcanics.

Acknowledgments

The seismic data are from the IRIS DMC. The authors would like to thank Dr. Peter M. Shearer and two anonymous reviewers for valuable comments; R.B. Herrmann and C.J. Ammon for the CPS package; Don Forsyth, and Yingjie Yang for the surface-wave code; Leland O'Driscoll for field efforts, and the PASSCAL Instrument Center. We acknowledge Matt Fouch for sharing the SKS splitting data. K.L. acknowledges Fenglin Niu and Iain Bailey for discussion on the surface wave and joint inversion codes, and Sally Thurner and Jen Gabler for manuscript editing. Figures were made by GMT (Wessel and Smith, 1991) and EarthVision™. This study was funded by NSF EarthScope grant EAR-0642474 and EAR-0746379.

Appendix A. Supplementary data

Supplementary data to this article can be found online at doi:10.1016/j.epsl.2012.01.020.

References

Atwater, T., 1970. Implications of plate tectonics for the Cenozoic tectonic evolution of western North America. Bull. Geol. Soc. Am. 81, 3513–3536.

Beaudoin, B.C., Godfrey, N.J., Klemperer, S.L., Lendl, C., Trehu, A.M., Henstock, T.J., Levander, A., Holl, J.E., Meltzer, A.S., Luetgert, J.H., Mooney, W.D., 1996. Transition from slab to slabless: results from the 1993 Mendocino Triple Junction seismic experiment. Geology 24, 195–199.

Beaudoin, B.C., Hole, J.A., Klemperer, S.L., Trehu, A.M., 1998. Location of the southern edge of the Gorda slab and evidence for an adjacent asthenospheric window: results from seismic profiling and gravity. J. Geophys. Res. Solid Earth 103, 30101–30115.

Bensen, G.D., Ritzwoller, M.H., Barmin, M.P., Levshin, A.L., Lin, F., Moschetti, M.P., Shapiro, N.M., Yang, Y., 2007. Processing seismic ambient noise data to obtain reliable broad-band surface wave dispersion measurements. Geophys. J. Int. 169, 1239–1260.

Benz, H.M., Zandt, G., Oppenheimer, D.H., 1992. Lithospheric structure of Northern California from teleseismic images of the upper mantle. J. Geophys. Res. Solid Earth 97, 4791–4807.

Blake, M.C., Jayko, A.S., McLaughlin, R.J., 1985. Tectonostratigraphic terranes of the northern Coast Ranges, California. ectonostratigraphic Terranes of the Circum-Pacific Region.

Blakely, R.J., Brocher, T.M., Wells, R.E., 2005. Subduction-zone magnetic anomalies and implications for hydrated forearc mantle. Geology 33, 445–448.

Bostock, M.G., Hyndman, R.D., Rondenay, S., Peacock, S.M., 2002. An inverted continental Moho and serpentinization of the forearc mantle. Nature 417, 536–538.

Brocher, T.M., Parsons, T., Trehu, A.M., Snelson, C.M., Fisher, M.A., 2003. Seismic evidence for widespread serpentinized forearc upper mantle along the Cascadia margin. Geology 31, 267–270.

Cole, R.B., Basu, A.R., 1995. Nd–Sr isotopic geochemistry and tectonics of ridge subduction and middle Cenozoic volcanism in western California. Geol. Soc. Am. Bull. 107, 167–179.

Dickinson, W.R., 1997. Tectonic implications of Cenozoic volcanism in coastal California. Geol. Soc. Am. Bull. 109, 936–954.

Dickinson, W.R., Snyder, W.S., 1979. Geometry of subducted slabs related to San Andreas transform. J. Geol. 87, 609–627.

Eakin, C.M., Obrebski, M., Allen, R.M., Boyarko, D.C., Brudzinski, M.R., Porritt, R., 2010. Seismic anisotropy beneath Cascadia and the Mendocino Triple Junction: interaction of the subducting slab with mantle flow. Earth Planet. Sci. Lett. 297, 627–632.

Forsyth, D.W., Li, A., 2005. Array analysis of two-dimensional variations in surface wave phase velocity and azimuthal anisotropy in the presence of multipathing interference. Seismic Earth: Array Analysis of Broadband Seismograms.

Fouch, M.J., West J.D., in preparation. The mantle flow field beneath the western United States.

Fulton, P.M., Saffer, D.M., 2009. Potential role of mantle-derived fluids in weakening the San Andreas Fault. J. Geophys. Res. Solid Earth 114.

Furlong, K.P., Govers, R., 1999. Ephemeral crustal thickening at a Triple Junction: the Mendocino crustal conveyor. Geology 27, 127–130.

Furlong, K.P., Schwartz, S.Y., 2004. Influence of the Mendocino Triple Junction on the tectonics of coastal California. Annu. Rev. Earth Planet. Sci. 32, 403–433.

Furlong, K.P., Lock, J., Guzofski, C., Whitlock, J., Benz, H., 2003. The Mendocino crustal conveyor: making and breaking the California crust. Int. Geol. Rev. 45, 767–779.

Godfrey, N.J., Klemperer, S.L., 1998. Ophiolitic basement to a forearc basin and implications for continental growth: the Coast Range Great Valley ophiolite, California. Tectonics 17, 558–570.

Godfrey, N.J., Beaudoin, B.C., Klemperer, S.L., 1997. Ophiolitic basement to the Great Valley forearc basin, California, from seismic and gravity data: implications for crustal growth at the North American continental margin. Geol. Soc. Am. Bull. 109, 1536–1562.

Grand, S.P., Helmberger, D.V., 1984. Upper mantle shear structure of North-America. Geophys. J. R. Astron. Soc. 76, 399–438.

Gulick, S.P.S., Meltzer, A.S., Henstock, T.J., Levander, A., 2001. Internal deformation of the southern Gorda plate: fragmentation of a weak plate near the Mendocino Triple Junction. Geology 29, 691–694.

Guzofski, C., Furlong, K.P., 2002. Migration of the Mendocino Triple Junction and ephemeral crustal deformation: implications for California Coast Range heat flow. Geophys. Res. Lett. 29, 12-1–12-4.

Hacker, B.R., Peacock, S.M., Abers, G.A., Holloway, S.D., 2003. Subduction factory, 2, Are intermediate-depth earthquakes in subducting slabs linked to metamorphic dehydration reactions? J. Geophys. Res. 108 (B1), 2030. doi:10.1029/2001JB001129.

Henstock, T.J., Levander, A., 2000. Lithospheric evolution in the wake of the Mendocino Triple Junction: structure of the San Andreas Fault system at 2 Ma. Geophys. J. Int. 140, 233–247.

Henstock, T.J., Levander, A., Hole, J.A., 1997. Deformation in the lower crust of the San Andreas fault system in northern California. Science 278, 650–653.

Herrmann, R.B., Ammon, C.J., 2002. Surface waves, receiver functions and crustal structure. Computer Program in Seismology.

Hole, J.A., Beaudoin, B.C., Henstock, T.J., 1998. Wide-angle seismic constraints on the evolution of the deep San Andreas plate boundary by Mendocino Triple Junction migration. Tectonics 17, 802–818.

Johnson, C.M., O'Neil, J.R., 1984. Triple junction magmatism: a geochemical study of Neogene volcanic rocks in western California. Earth Planet. Sci. Lett. 71, 241–262.

Julia, J., Ammon, C.J., Herrmann, R.B., Correig, A.M., 2000. Joint inversion of receiver function and surface wave dispersion observations. Geophys. J. Int. 143, 99–112.

Kawakatsu, H., Kumar, P., Takei, Y., Shinohara, M., Kanazawa, T., Araki, E., Suyehiro, K., 2009. Seismic evidence for sharp lithosphere–asthenosphere boundaries of oceanic plates. Science 324, 499–502.

Lachenbruch, A.H., Sass, J.H., 1980. Heat-Flow and Energetics of the San-Andreas Fault Zone. J. Geophys. Res. 85, 6185–6222.

Leeman, W.P., Lewis, J.F., Evarts, R.C., Conrey, R.M., Streck, M.J., 2005. Petrologic constraints on the thermal structure of the Cascades arc. J. Volcanol. Geotherm. Res. 140, 67–105.

Levander, A., Henstock, T.J., Meltzer, A.S., Beaudoin, B.C., Trehu, A.M., Klemperer, S.L., 1998. Fluids in the lower crust following Mendocino Triple Junction migration: active basaltic intrusion? Geology 26, 171–174.

Li, X.Q., Yuan, X.H., Kind, R., 2007. The lithosphere–asthenosphere boundary beneath the western United States. Geophys. J. Int. 170, 700–710.

Ligorria, J.P., Ammon, C.J., 1999. Iterative deconvolution and receiver–function estimation. Bull. Seismol. Soc. Am. 89, 1395–1400.

Liu, K.H., 2009. NA-SWS-1.1: a uniform database of teleseismic shear wave splitting measurements for North America. Geochem. Geophys. Geosyst. 10.

Liu, M., Furlong, K.P., 1992. Cenozoic volcanism in the California Coast Ranges—numerical-solutions. J. Geophys. Res. Solid Earth 97, 4941–4951.

Liu, K., Levander, A., Niu, F., Miller, M.S., 2011. Imaging crustal and upper mantle structure beneath the Colorado Plateau using finite frequency Rayleigh wave tomography. Geochem. Geophys. Geosyst. 12, Q07001. doi:10.1029/2011GC003611.

Obrebski, M., Allen, R.M., Xue, M., Hung, S.H., 2010. Slab–plume interaction beneath the Pacific Northwest. Geophys. Res. Lett. 37.

Piromallo, C., Becker, T.W., Funiciello, F., Faccenna, C., 2006. Three-dimensional instantaneous mantle flow induced by subduction. Geophys. Res. Lett. 33, L08304. doi:10.1029/2005GL025390.

Porritt, R.W., Allen, R.M., Boyarko, D.C., Brudzinski, M.R., 2011. Investigation of Cascadia segmentation with ambient noise tomography. Earth Planet. Sci. Lett. 309, 67–76.

Rondenay, S., 2009. Upper mantle imaging with array recordings of converted and scattered teleseismic waves. Surv. Geophys. 30, 377–405.

Schmandt, B., Humphreys, E., 2010. Complex subduction and small-scale convection revealed by body-wave tomography of the western United States upper mantle. Earth Planet. Sci. Lett. 297, 435–445.

Schmitt, A.K., Romer, R.L., Stimac, J.A., 2006. Geochemistry of volcanic rocks from the Geysers geothermal area, California Coast Ranges. Lithos 87, 80–103.

Shapiro, N.M., Campillo, M., Stehly, L., Ritzwoller, M.H., 2005. High-resolution surface-wave tomography from ambient seismic noise. Science 307, 1615–1618.

Snieder, R., 2004. Extracting the Green's function from the correlation of coda waves: a derivation based on stationary phase. Phys. Rev. E 69.

Thurber, C., Zhang, H.J., Brocher, T., Langenheim, V., 2009. Regional three-dimensional seismic velocity model of the crust and uppermost mantle of northern California. J. Geophys. Res. Solid Earth 114.

Whitlock, J.S., Furlong, K.P., Lesher, C.E., Furman, T., 2001. The Juan de Fuca Slab-window and Coast Range Volcanics, California: correlation between subducted slab age and mantle wedge geochemistry. EOS Trans. Am. Geophys. Union 82, F1186 (Abstr.).

Wilson, D.S., 1986. A kinematic model for the Gorda deformation zone as a diffuse southern boundary of the Juan de Fuca plate. J. Geophys. Res. 91, 10 259–10 269.

Wilson, D.S., 1989. Deformation of the so-called Gorda plate. J. Geophys. Res. 94, 3065–3075.

Yang, Y.J., Forsyth, D.W., 2006. Regional tomographic inversion of the amplitude and phase of Rayleigh waves with 2-D sensitivity kernels. Geophys. J. Int. 166, 1148–1160.

Yang, Y., Ritzwoller, M.H., Lin, F.-C., Moschetti, M.P., Shapiro, N.M., 2008. Structure of the crust and uppermost mantle beneath the western United States revealed by ambient noise and earthquake tomography. J. Geophys. Res. 113, B12310. doi:10.1029/2008JB005833.

Yao, H.J., van der Hilst, R.D., de Hoop, M.V., 2006. Surface-wave array tomography in SE Tibet from ambient seismic noise and two-station analysis—I. Phase velocity maps. Geophys. J. Int. 166, 732–744.

Zandt, G., Furlong, K.P., 1982. Evolution and thickness of the lithosphere beneath coastal California. Geology 10, 376–381.

Zandt, G., Humphreys, E., 2008. Toroidal mantle flow through the western US slab window. Geology 36, 295–298.

Zhai, Y., 2010. The lithospheric structure of the Mendocino Triple Junction: implications of receiver function analysis. Master thesis, Rice University.

Zucca, J.J., Fuis, G.S., Milkereit, B., Mooney, W.D., Catchings, R.D., 1986. Crustal Structure of Northeastern California. J. Geophys. Res. Solid 91, 7359–7382.